Environmental Pollution 254 (2019) 112848

Contents lists available at ScienceDirect

Environmental Pollution

journal homepage: www.elsevier.com/locate/envpol

Source Apportionment of Volatile Organic Compounds (VOCs) by Positive Matrix Factorization (PMF) supported by Model Simulation and Source Markers - Using Petrochemical Emissions as a Showcase☆

Yuan-Chang Su [a], Wei-Hao Chen [a], Chen-Lun Fan [a], Yu-Huei Tong [a], Tzu-Hsiang Weng [a], Sheng-Po Chen [b], Cheng-Pin Kuo [a], Jia-Lin Wang [c, *], Julius S. Chang [b]

[a] Environmental Simulation CO. LTD., Taiwan
[b] Atmospheric Sciences Research Center, University at Albany, SUNY, USA
[c] Department of Chemistry, National Central University, Taiwan

ARTICLE INFO

Article history:
Received 27 March 2019
Received in revised form
24 June 2019
Accepted 4 July 2019
Available online 8 August 2019

Keywords:
Source-receptor
Petrochemical complex
Photochemical assessment measurement stations (PAMS)

ABSTRACT

This study demonstrates the use of positive matrix factorization (PMF) in a region with a major Petrochemical Complex, a prominent source of volatile organic compounds (VOCs), as a showcase of PMF applications. The PMF analysis fully exploited the quality and quantity of the observation data, sufficed by a cluster of 9 monitoring sites within a 20 km radius of the petro-complex. Each site provided continuous data of 54 speciated VOCs and meteorological variables. Wind characteristics were highly seasonal and played a decisive role in the source-receptor relationship, hence the dataset was divided into three subsets in accordance with the prevailing wind flows. A full year of real-time data were analyzed by PMF to resolve into various distinct source types including petrochemical, urban, evaporative, long-range air parcels, etc., with some sites receiving more petro-influence than others. To minimize subjectivity in the assignment of the PMF source factors, as commonly seen in some PMF works, this study attempted to solidify PMF results by supporting with two tools of spatially/temporally resolved air-quality model simulations and observation data. By exploiting the two supporting tools, the dynamic process of individual sources to a receptor were rationalized. Percent contributions from these sources to the receptor sites were calculated by summing over the occurrence of different source types. Interestingly, although the Petro-complex is the single largest local VOC source in the 20 km radius study domain, all monitoring sites in the region received far less influence from the Petro-complex than from other emission types within or outside the region, which together add up to more than 70% of the total VOC abundance.

1. Introduction

Volatile organic compounds (VOCs) from anthropogenic sources are often associated with issues of toxicity (Hsu et al., 2018; Jones, 1999; Lau et al., 1997; Simpson et al., 2013; Zhang et al., 2013), formation of tropospheric ozone (Atkinson and Arey, 2003; Carter, 1990, 1994), secondary organic aerosols (SOA) (McFiggans et al., 2019; Schauer et al., 2002; Seagrave et al., 2006), among others. The presence of atmospheric VOCs arises from a variety of sources of either anthropogenic or biogenic nature. Of these primary sources, the petrochemical industry receives great attention due to its significant and localized release of reactive VOCs to the atmosphere (Hajizadeh et al., 2018; Han et al., 2018; Ryerson et al., 2003). To permit quantitative assessment of the impact, emissions from the petro-industry must be effectively differentiated from other notable sources with sufficient specificity and unambiguity. Studies of a pronounced source affecting surrounding environments have been investigated in the past. Analysis with a large number of passive sampling canisters was commonly used to recognize the composition or spatial distribution of VOCs around the industrial complex (Cetin et al., 2003; Dumanoglu et al., 2014; Mo et al., 2015; Pekey and Yılmaz, 2011; Ras et al., 2009; Wang et al., 2018; Wei et al., 2014). The approach of incorporating observations at downwind sites coupled with receptor modeling is an effective way to estimate the contribution from the target emission source (Brown

☆ This Paper has been recommended for acceptance by Admir Créso Targino.
* Corresponding author. Department of Chemistry, National Central University, Chungli 320, Taiwan.
E-mail address: cwang@cc.ncu.edu.tw (J.-L. Wang).

https://doi.org/10.1016/j.envpol.2019.07.016
0269-7491/

et al., 2007; Buzcu-Guven and Fraser, 2008; Buzcu and Fraser, 2006; Leuchner and Rappenglück, 2010; Xie and Berkowitz, 2006). Measurement of petrochemical specific species by optical instruments can be used to investigate the influences form fugitive emissions. (Chen et al., 2014a; Wu et al., 2014; Yang et al., 2016; Zhou et al., 2019). However, while these cases may have shown their own merits, to pin down emissions that can be unambiguously linked to the particularly source is often limited by the insufficient representative chemical markers or monitoring capabilities, rendering assessment incomplete or with large uncertainty. To reduce uncertainty and increase specificity, certain criteria are helpful when it comes to making results more revealing and less ambiguous. These criteria may include, for instance: 1. Emissions are intrinsically pronounced, 2. Source signatures can be found with unique features, 3. Monitoring capabilities are highly speciated and with sufficient temporal and spatial resolution, 4. Data resolving tools are available to divulge embedded characteristic signals. To test the idea of effective differentiation, a Petrochemical Complex was chosen as the pronounced source of VOCs to fulfill the aforementioned first three criteria. The Petrochemical Complex, hereafter dubbed Petro-complex, is the 6th largest petrochemical industrial complex in the world (Formosa Plastics Group, 2013). It is located on the western coast of central Taiwan. Because of the sheer size and potential impact on air quality in the region, a network of nine air-quality monitoring stations within a radius of 20 km of the Petro-complex was established to provide hourly measurements of relevant organic species. Because the scale of the monitoring capability in terms of the number of organic species, area coverage and time resolution is mostly likely unpresented worldwide, a solid groundwork is laid for data deciphering with proper tools.

In our previous study, it has been demonstrated successfully that the provision of the monitoring network around a Petro-complex facilitated tracking the emission footprints on neighboring areas (Su et al., 2016). Although the simple fingerprinting method has shown great usefulness to assess influence in a qualitative manner, it lacks the ability to provide area-specific loading (magnitude) information. As a result, quantification of emission impact on a receptor area from a specific source has not been achieved. One approach to obtain this quantitative information is the use of receptor-based source apportionment models, such as Chemical Mass Balance (CMB) (Cooper and Watson, 1980) and Positive Matrix Factorization (PMF) (Paatero and Tapper, 1994). In general, when complete emission profiles are not available, the PMF model is more desired to identify contributing factors. In this study, PMF is used to resolve and quantify contributions from relevant sources in the region, including the seemingly single most prominent VOC source in the region, the Petro-complex, as a test bed for the integrated approach of source differentiation and apportionment.

With the PMF results available, the understanding of the source-and-receptor relationship in the region was further enhanced by three-dimensional air-quality modeling along with unique features of the time-series data to provide pictorial illustration of air flow dynamics. The use of air-quality modeling to support PMF adds another depth in the interpretation of the PMF results, since the transport process of pollutants as plumes which is not given by PMF can be visualized by model simulation and also supported by unique time-resolved features embedded in the data.

2. Materials and methods

2.1. Description of VOC monitoring sites and measurement method

The Petro-complex occupies an area of 7.5 km × 4.5 km (2255 ha). Extending outwards to 20 km radius from the Petro-complex forms the study region on the west coast of Taiwan, hereafter dubbed “Petro-region”. Nine photochemical assessment monitoring stations (PAMS) were setup within the Petro-region since 2013 (Fig. 1). The distances between neighboring stations were 5–10 km. All PAMS sites also measured meteorological parameters (temperature, humidity, rainfall, wind speed and wind direction). Site F1 was within the campus of Petro-complex, other eight sites (F2 ~ F9) were on the rooftop of two to three-story buildings (inlet height = 10–18 m) in the surrounding areas to monitor plumes in different wind directions. To simply illustration, only the data of F2, F4 and F9 were discussed to represent the north, south and east directions of the Petro-chemical complex, respectively.

Other than the Petro-complex, there were no prominent local emission sources in this area due to the extremely rural setting. Thus, the VOC abundance was expected to be contributed by the Petro-complex and sources outside the Petro-region.

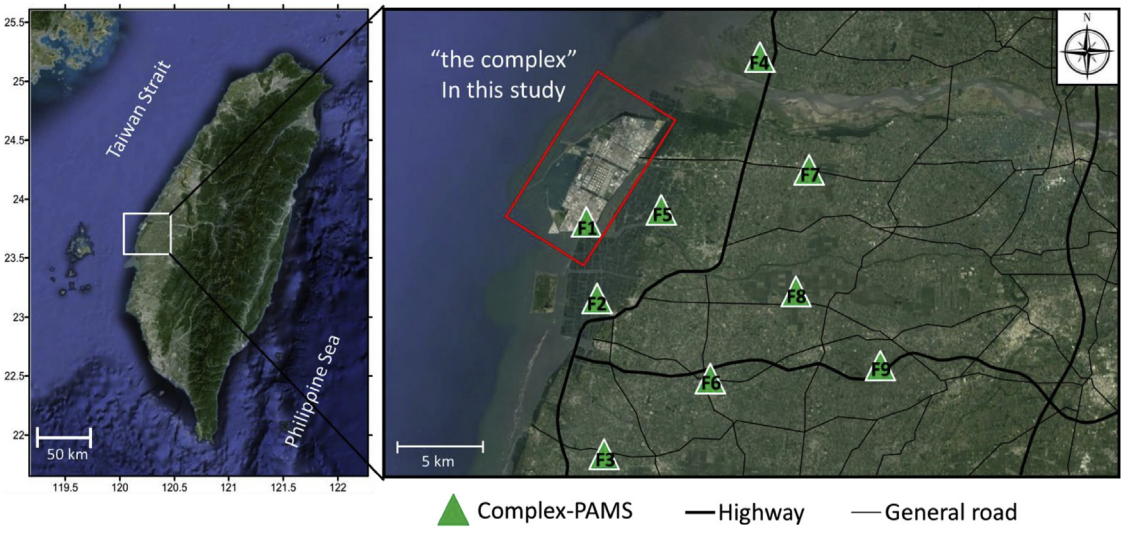

Fig. 1. Locations of nine PAMS sites surrounding the Petro-complex (red box) as shown by the triangles. The Petro-region (white box) has a radius of approximately 20 km from the Petro-complex.

At all PAMS sites, commercial automated gas chromatographs (called auto-GCs provided by Perkin Elmer, USA) equipped with dual columns/dual flame ionization detectors, coupled with a cryogen-free thermal desorption unit, were employed to provide hourly measurements of 54 VOCs from C_2–C_{11}. All 54 species were calibrated by a commercial standard gas mixture (Spectra gases, NJ, USA) at sub-ppb levels with measurement detection limits (MDL) shown in Table 1. The sum of the 54 species can represent as much as 70% the total VOC level in an urban setting due mostly to vehicular emissions, but could be slightly lower in an industrial setting where traffic is not the only major source refinery (Chen et al., 2014b; Su et al., 2016). Each daily batch of 24-h measurements comprised one calibration check, one blank (high-purity nitrogen) and 22 ambient sample injections. Quality assurance and control were performed on the daily basis. Each month the control charts of the standard gas and blank injections were checked to inspect for stability of the auto-GCs overtime. The PAMS's hourly data were used in two ways; either as total concentrations called PAMS-TVOCs, defined as the summed mixing ratios of the 54 target VOCs, or as individual speciated mixing ratios. More information and measurement details can be found in our previous published work (Su et al., 2016).

2.2. Model simulation setup

The Fifth-Generation Penn State/NCAR Mesoscale Model (MM5) and the three-dimensional Eulerian Air-Quality Model specific to PAMS species (PAMS-AQM) were used for meteorological and air quality simulations (Chen et al., 2010). The horizontal grid sizes for the nested domains are $81 \times 81\ km^2$ (D1), $27 \times 27\ km^2$ (D2), $9 \times 9\ km^2$ (D3) and $3 \times 3\ km^2$ (D4). There were a total of 15 non-uniform sigma levels in the vertical direction from the surface to approximately 13.5 km above the surface, with the lowest level of approximately 20 m in height. The MM5 meteorological simulation results with updated land-use database (Lin, 2012) are the dynamic field inputs for the transport chemical model, i.e., PAMS-AQM (Chen et al., 2010), which is used to simulate the evolution of PAMS organics, radicals and oxidants in the atmosphere. The Regional Acid Deposition Model, version 2 (RADM2) chemical mechanism (Stockwell et al., 1990) is used to simulate radicals and oxidants, whereas the PAMS diagnostic chemical mechanism is used for PAMS individual species. The chemical transformation, atmospheric transport and mixing, sources and deposition processes of each PAMS species were calculated separately. Details of PAMS-AQM model structures can be found in our previous publication (Chen et al., 2010; Chen et al., 2014c; Chen et al., 2015).

Anthropogenic and biogenic emissions for East Asia are derived from the Asia emission inventory by INTEX B 2006 (Li et al., 2014; Zhang et al., 2009). Further detailed anthropogenic emissions are derived from the Taiwan Emission Database System (TEDS Version 8.1) (Taiwan-EPA, 2011), and the biogenic emissions are obtained from the Taiwan Biogenic Emission Inventory System (TBEIS) (Chang et al., 2005).

2.3. PMF model description

The principle and detailed description of the PMF model can be referred to studies by Paatero (1997); Paatero and Tapper (1994). In recent years, PMF has been widely applied as a useful tool to resolve VOC source-receptor relationships and assess the contributions from different emission sources to establish a control strategy (Brown et al., 2007; Buzcu-Guven and Fraser, 2008; Buzcu and Fraser, 2006; Cai et al., 2010; Guo et al., 2011; Leuchner and Rappenglück, 2010; McCarthy et al., 2013; Saeaw and Thepanondh, 2015; Stojić et al., 2015; Wei et al., 2014; Xie and Berkowitz, 2006; Yuan et al., 2013; Zhang et al., 2015). Furthermore, the modified PMF model was developed to quantify contributions from sources of $PM_{2.5}$ and VOCs (Kuo et al., 2014; Liao et al., 2013).

In PMF model, a data matrix X_{ij} represents the VOC

Table 1
Target VOCs measured by Complex-PAMS and their measurement detection limits (MDLs).

Category	No.	Compound name	CN*	MDL (ppbv)	Category	No.	Compound name	CN	MDL (ppbv)
Alkanes	1	ethane	2	0.19	Alkynes	29	acetylene	2	0.18
	2	propane	3	0.21					
	3	isobutane	4	0.04	Alkenes	30	ethylene	2	0.17
	4	n-butane	4	0.08		31	propylene	3	0.07
	5	cyclopentane	5	0.04		32	t-2-butene	4	0.07
	6	isopentane	5	0.07		33	1-butene	4	0.09
	7	n-pentane	5	0.07		34	c-2-butene	4	0.06
	8	2,2-dimethylbutane	6	0.05		35	t-2-pentene	5	0.07
	9	2,3-dimethylbutane	6	0.02		36	1-pentene	5	0.05
	10	2-methylpentane	6	0.04		37	c-2-pentene	5	0.07
	11	3-methylpentane	6	0.07		38	isoprene	5	0.06
	12	n-hexane	6	0.04					
	13	methylcyclopentane	6	0.02	Aromatics	39	benzene	6	0.06
	14	2,4-dimethylpentane	7	0.07		40	toluene	7	0.03
	15	cyclohexane	6	0.06		41	ethylbenzene	8	0.03
	16	2,3-dimethylpentane	7	0.02		42	m,p-xylene	8	0.02
	17	2,3-dimethylpentane	7	0.04		43	styrene	8	0.04
	18	3-methylhexane	7	0.05		44	o-xylene	8	0.02
	19	2,2,4-trimethylpentane	8	0.03		45	isopropylbenzene	9	0.02
	20	n-heptane	7	0.04		46	n-propylbenzene	9	0.02
	21	methylcyclohexane	7	0.04		47	m-ethyltoluene	9	0.02
	22	2,3,4-trimethylpentane	8	0.03		48	p-ethyltoluene	9	0.04
	23	2-methylheptane	8	0.02		49	1,3,5-trimethylbenzene	9	0.02
	24	3-methylheptane	8	0.02		50	o-ethyltoluene	9	0.02
	25	n-octane	8	0.03		51	1,2,4-trimethylbenzene	9	0.03
	26	n-nonane	9	0.02		52	1,2,3-trimethylbenzene	9	0.04
	27	n-decane	10	0.02		53	m-diethylbenzene	10	0.03
	28	n-undecane	11	0.02		54	p-diethylbenzene	10	0.02

CN* stands for the number of carbons for a given compound.

concentration of j-th species measured in i-th sample provided by the measurements, the PMF algorithm then determine the following parameters of (1) the number of VOC source factors (p), (2) the chemical composition profile of each source factor F, (3) the contribution of each source factor to each sample G, and (4) the residual matrix of each species to each sample e_{ij}. The relationship can be expressed by equation (1):

$$X_{ij} = \sum_{k=1}^{p} G_{ik} F_{kj} + e_{ij} \quad (1)$$

The objective is to minimize function Q defined by equation (2), where n and m are the number of samples and the number of VOC species, s_{ij} is the uncertainty of X_{ij}:

$$Q = \sum_{i=1}^{n} \sum_{j=1}^{m} \frac{e_{ij}^2}{s_{ij}^2} \quad (2)$$

The constraints for equations (1) and (2) are that the contribution G and source factor F should be non-negative to be physically meaningful.

2.4. PMF model implementation

The EPA PMF 5.0 receptor model was employed in this study. Input data files contain two matrices, the measured species concentration (X_{ij}) and uncertainty (U_{ij}). The uncertainty was calculated by species concentrations and method detection limit (MDL_j) of each species. If the species concentration was above the MDL_j, the uncertainty were set as:

$$U_{ij} = \sqrt{(0.5 \times MDL_j)^2 + (\text{error fraction} \times X_{ij})^2}$$

; if species concentration was below the MDL_j, concentration was replaced by 1/2 MDL_j, and the uncertainties were set as 5/6 MDL_j (Kuo et al., 2014; Reff et al., 2007). Missing values were excluded from entire sample. Other uncertainty estimating methods were also examined (Poirot et al., 2001; Reff et al., 2007), but there is no significant change for PMF results.

In most cases, species of PAMS with low S/N and a high percentage of data below the detection limit did not give rise to enough variability in concentrations to contribute to factor identification in a significant way. Therefore, for those species whose abundance was lower than 0.2 for the signal-to-noise (S/N) level or smaller than MDL_s for over 80% of the measurements, they were excluded from PMF analysis (status code = bad). For the species that had less than twice the S/N ratios or smaller than $MDLs$ over 20% of the measurements, they were down-weighted by a factor of three (status code = weak). The PMF input data statistics and status code under different wind patterns at each site for each VOC species are presented in supplementary material (Tables S1–S3).

To determine the optimal number of source types under different wind patterns at each site, 3–8 source factors were examined. The model was run 20 times with a random seed to determine the stability of Q values and the resulting source profiles can be physically interpreted. In this study, on average, approximately 98% of the scaled residuals calculated by PMF were between −3 and 3, indicating a good fit of the modeled results (Buzcu and Fraser, 2006).

2.5. Wind field characteristics

Source apportionment of the hourly mixing ratios of the 54 PAMS VOC species from three sites (F2, F4, and F9) were analyzed by PMF to simply illustration, since these three sites represent general areas in the south, north and farthest east of the Petro-complex. The time-series data of other sites were used to assist divulging the transport of plumes within the Petro-region. Furthermore, because the wind field in the region is highly seasonal, greatly affecting the transport routes of air pollutants (Su et al., 2016), the whole year data were divided into three sub-sets for PMF analysis in accordance with the distinct wind patterns in the Petro-region: northeast monsoonal (NEM) flow (135 days), southwest monsoonal (SWM) flow (31 days), and local circulation/diffusion (LCD) (105 days) (Chen et al., 2018). For the remaining days, the wind types were too vague (such as typhoon or ambiguous wind fields) to be clearly categorized, and hence not included in the assessment.

3. PMF results validated by simulation and real-time measurement

3.1. NEM flows

Under the NEM flows mostly during colder months, almost all the wind directions at each site were between 315 and 45°, thus minimal influence from the Petro-complex would affect sites of F4 ~ F9, which were on the east side of the Petro-complex (Su et al., 2016). By comparison, the F2 site would be more affected by the Petro-complex's emissions. Source composition profiles for the five factors resolved by PMF at site F2 are shown in Fig. 2.

These five factors, largely representing source signatures, can be assigned based on prior knowledge and specific source markers. Profile A (Fig. 2a) mainly consists of longer-lived species among the measured VOCs such as ethane (No. 1, 1.81 ppbv, accounting for 77% of the total ethane abundance), propane (No. 2, 0.77 ppbv, 63%), acetylene (No. 29, 0.68 ppbv, 75%) and benzene (No. 39, 0.22 ppbv, 68%). This profile revealing longer-lived/less reactive VOC species (such as alkanes) than the reactive ones (such as alkenes) indicate that the VOC sources that shaped Profile A may be transported from afar and thus the more reactive compounds became relatively less abundant. Moreover, the toluene to benzene (T/B) ratio, which is a common indicator of aged air mass, was rather low ($\leqq 1$), suggesting that these air parcels were relatively photochemically aged and the sources were likely to lie outside the Petro-region (Gelencsér et al., 1997; Miller et al., 2011; Pekey and Yılmaz, 2011; Zhang et al., 2013).

Profile B (Fig. 2b) exhibits high mixing ratios of toluene (No. 40, 0.76 ppbv, 74%) and other aromatics such as ethylbenzene (No. 41, 0.04 ppbv, 37%), m, p-xylene (No. 42, 0.15 ppbv, 60%), and o-xylene (No. 44, 0.06 ppbv, 56%). Besides those aromatics, small amounts (10–30%) of alkanes, alkenes, and acetylene were also noticed. This profile may imply that VOC contribution was mainly shaped by industrial and painting solvents (Scheff and Wadden, 1993; Scheff et al., 1989; Yuan et al., 2010), as well as contribution from traffic and urban emissions (Chan et al., 2006; Scheff and Wadden, 1993; Scheff et al., 1989). The determination was also supported by the rather high T/B ratio of 18.9, in between the traffic emission (T/B ≒ 2) and chemicals and painting industries (T/B > 30) (Pekey and Yılmaz, 2011). Other useful emission markers include the use of ratios ethylene/acetylene (E/A) and propylene/acetylene (P/A). Su et al. (Su et al., 2016) found the E/A and P/A ratios higher than 3.0 and 1.5 are positive indication of refinery emissions which can effectively separate emissions from on-road traffic. Herein, the E/A ratio showed a relatively low value of 0.96, indicating the low likelihood of the air parcels ever influenced by Petro-complex (Su et al., 2016), but rather from the urban environment dominated by traffic emissions.

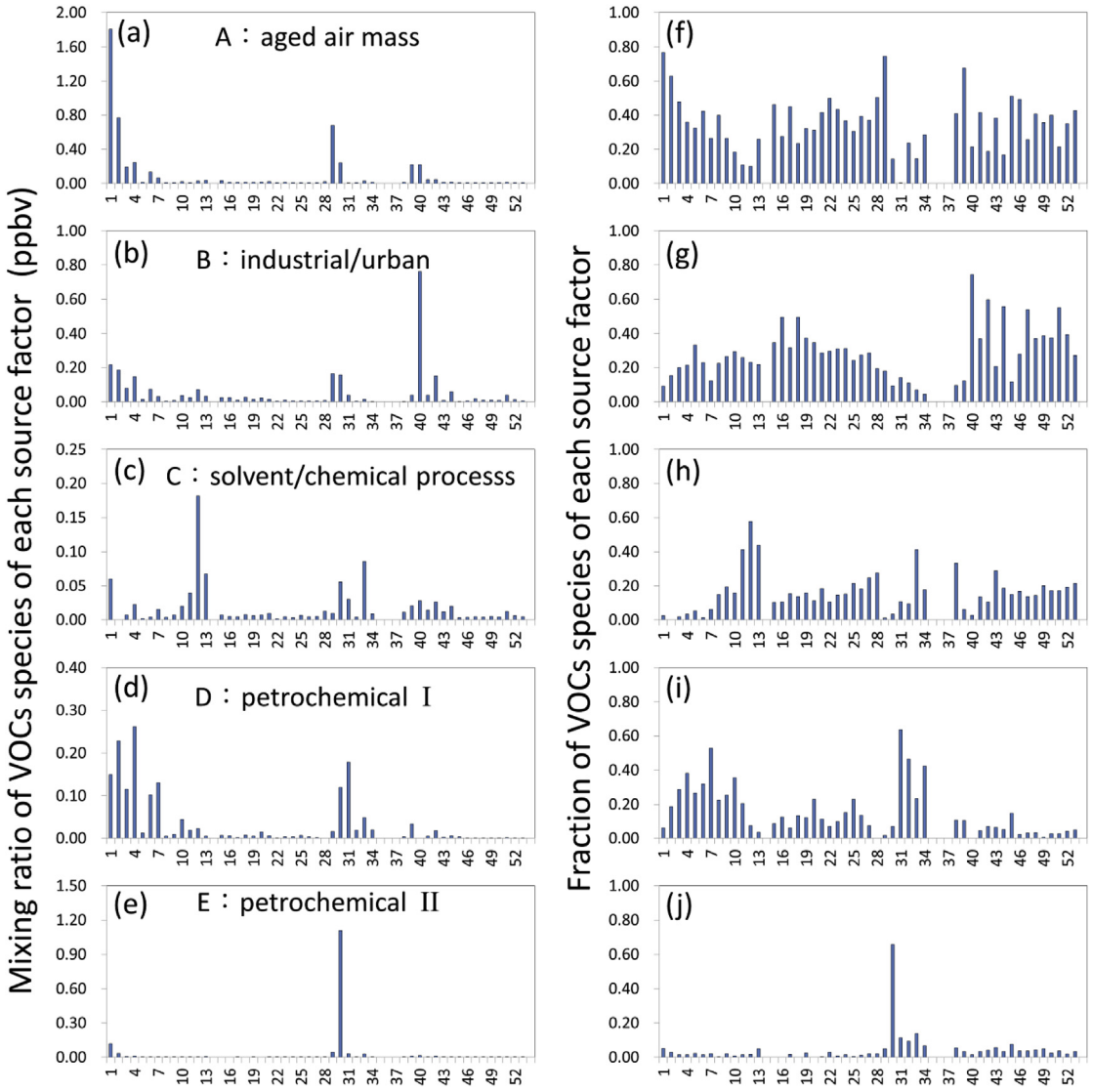

Fig. 2. Compositional profiles for the five factors resolved by PMF at site F2 under NEM flows. Left panels from (a) to (e): aged air, industrial/urban, solvent/chemical processes, petrochemical I, and petrochemical II, respectively, in mixing ratios (ppbv); right panels from (f) to (j) correspond to the left panels, showing the relative fraction of each species to its total abundance. Numbers on the abscissa correspond to the species No. listed in Table 1.

Profile C (Fig. 2c) is accentuated by the significant contribution of n-hexane (No. 12, 0.18 ppbv, 58%), methylcyclopentane (No.13, 0.07 ppbv, 44%), 1-butene (No.33, 0.09 ppbv, 41%), and sorts of alkenes. This composition can be defined as solvent usage or chemical processes (Buzcu and Fraser, 2006).

Profile D (Fig. 2d) mainly consists of C3–C5 alkanes, such as propane (No. 2, 0.23 ppbv, 19%), isobutene (No. 3, 0.12 ppbv, 29%), n-butene (No. 4, 0.26 ppbv, 38%), isopentane (No. 6, 0.10 ppbv, 32%), and n-pentane (No.7, 0.13 ppbv, 53%). In addition, the high level of propylene (No. 31, 0.18 ppbv, 64%) contributing to a P/A ratio 7.5 gave an indication of refinery (Chen et al., 2014b; Su et al., 2016). The Petro-complex is known for its large refinery capacity, along with its downstream plastic industries in the complex. Thus, this distinct composition has strong linkage to the Petro-complex, and is defined as the petrochemical-I (Buzcu and Fraser, 2006; Leuchner and Rappenglück, 2010; Scheff and Wadden, 1993; Wei et al., 2014). Likewise, Profile E (Fig. 2e), as represented by a single dominant compound of ethylene (No.30, 1.1 ppbv, 66%), which along with propylene are the two prominent products of refinery, can also be ambiguously assigned as the petrochemical-II (Buzcu and Fraser, 2006; Jobson et al., 2004; Leuchner and Rappenglück, 2010; Scheff and Wadden, 1993; Su et al., 2016; Wei et al., 2014). The reason that ethylene and propylene did not appear in proportion despite their common refinery nature is due to the different locations of the facilities within the rather large campus of Petro-complex relative to the study domain.

As the seasonal NEM flows prevailed, the monotonous wind characteristics prevented the petro-emissions from hardly being blown to the inland area (eastward of the Petro-region). Such a geo-meteorological characteristic is consistent with the PMF results. The measurement data of site F9 resolved by PMF gave rise to four factors (profile F, G, H, and I), as shown in Fig. 3. Profile F, G, and H (Fig. 3a, b, 3c) are labeled as “aged”, “industrial/urban” and “solvent/chemical”, respectively, similar to Profile A, B, and C. However, significant differences were noticed between Profile I (Fig. 3d) and Profile D/E. Profile I mainly consists of alkanes, small amounts (10–30%) of alkenes, acetylene and aromatics. The ratio of toluene/benzene of approximately 1.9 is close to that of the car exhaust signature, and the overall speciation profile is also consistent with vehicle fuel evaporation (Brown et al., 2007; Scheff and Wadden,

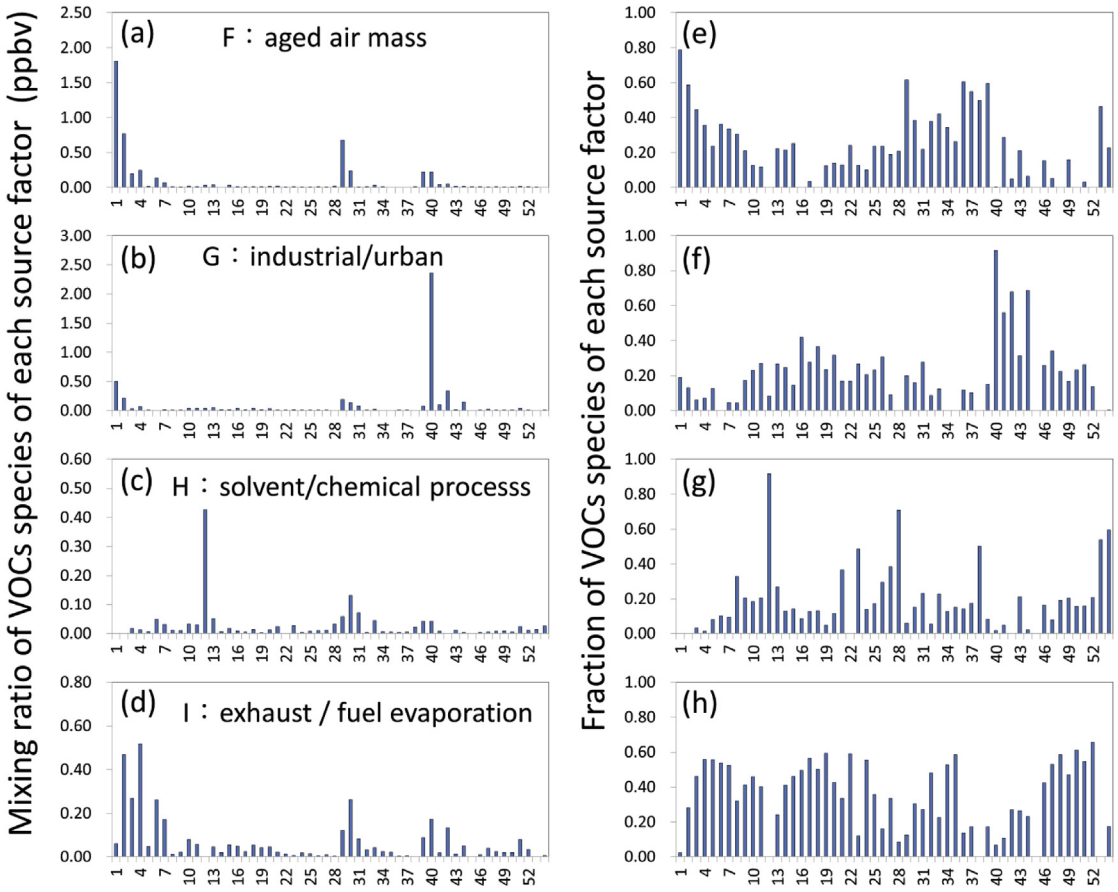

Fig. 3. Compositional profiles for the four factors resolved by PMF analysis at site F9 under the NEM flows, and no petrochemical signals were resolved. Left panels from (a) to (d): aged air, industrial/urban, solvent/chemical processes and exhaust/fuel evaporation, respectively, in mixing ratios (ppbv); right panels from (e) to (h) correspond to the left panels, showing the relative fraction of each species to its total abundance. Numbers on the abscissa correspond to the species No. listed in Table 1.

1993). Furthermore, very similar VOC speciation profile to the findings of tunnel experiments was also noticed (Ho et al., 2009; Hwa et al., 2002; Liu et al., 2014). As a result, Profile I is defined as car exhaust/fuel evaporation. Different from F2, no petrochemical signatures (I and II) were identified for F9.

The PMF results of site F4 was found to be similar to F9 and; therefore, the sources were labeled accordingly as aged, industrial/urban and solvent/chemical. No petrochemical signatures were found for site F4 either, since it was now in the upwind direction of the Petro-complex. Under the NEM flows, the sites on the north and east side of the Petro-region received minimal influence from the Petro-complex, and only site F2, located at the direct downwind of the Petro-complex in the south, revealed strong signatures of petrochemical I and II. As a result, the downwind-upwind relationship was strongly determined by the wind flows.

Although the PMF resolved source factors mentioned above have been assigned with source types based on the existing knowledge, the assignment did not rule out the likelihood of subjectivity. Therefore, two supporting tools, PAMS-AQM model simulation and site-specific hourly monitoring data, were used here to examine the robustness of the source assignment resulted from PMF. Even though the NEM is dominated by the northeasterly wind in the Petro-region, a slightly swing in the wind angle from northwest to northeast does occur and can alter the source types affecting the Petro-region, displaying multiple facets in the source-receptor relationship in the region. Two typical cases are displayed as follows.

In one typical case, the entire Petro-region was overwhelmed by the long-range air parcels. Fig. 4 shows the simulations of total quantifiable VOCs by PAMS (PAMS-TVOCs) under the NEM flows. The air brought down by very strong northeasterly winds with wind speed over 6 m/s was laden with pollutants from the northern major cities of the island (including Taipei) with multi-million population to affect downwind Petro-region. Outside the island, the outflows from the Asian continent also elevated the baseline level. These two sources combined affected the downwind coastal areas including the Petro-region, as seen in Fig. 4. Modeling was able to reproduce the PAMS-TVOC level in agreement with the PAMS observations (supplementary material Fig. S1). In this particular case, the VOC compositional profiles at all sites were extremely similar to Profile A using site F2 as an illustration (Fig. 5a). In this particular case, Profile A as the aged air mass from long-range transport can be clearly resolved from other source types by PMF and played the dominant factor affecting the Petro-region (Fig. 5b). In another NEM case (supplementary material Fig. S4), when the wind speed over the land surface significantly decreased (1–2 m/s), the urban plumes from a nearby metropolitan area in the adjacent north became influential. In this case, urban signatures can be easily extracted by PMF. The close agreement between simulations and observations is shown in the supplementary material Fig. S2. In this case of northern urban influence, the observed speciated profile at the receptor sites F2 was extremely similar to Profile B as shown in Fig. S5a. The urban influence dominated the PAMS-TVOC abundance in the morning of 1/17, but decreased abruptly in the afternoon as the wind direction slightly changed and the urban influence shifted away from the F2

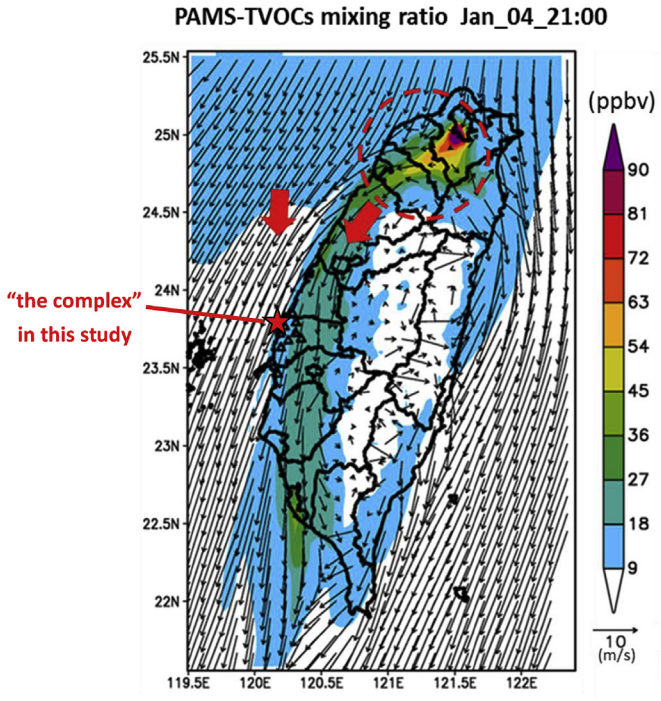

Fig. 4. A typical case of PAMS-TVOC surface-level simulations under NEM flows. The dashed red circle indicates the elevated VOC mixing ratios over the area of Taipei (the largest metropolis on the island), and the two arrows indicate the urban plumes and upstream continental outflows from afar, respectively.

site (Fig. S5b). The integrated utilization of model simulations, real-time VOC observations and PMF analysis successfully illustrated the dynamic process of individual sources affecting the receptor site.

3.2. SWM flows

Under the SWM flows, since wind direction in the Petro-region was mostly between 135 and 225°, hence emissions from the Petro-complex hardly influenced all stations except site F4. The observed mixing ratios of PAMS-TVOCs at F4 increased when it was directly at the downwind direction of the Petro-complex (Fig. 6a). At site F4, seven emission factors (seen in supplementary material Fig. S3) are resolved by PMF; they are aged air mass (similar to profile A), industry/urban (similar to profile B), petrochemical-I, petrochemical-II (similar to profile D and E), exhaust/fuel evaporation (similar to profile I), as well as biogenic and local painting. The two assisting tools of PMF validation were again applied to solidify the source assignment of the PMF factors. Site F4 was found to be most influenced by the two petrochemical emission factors, which is very sensitive to wind direction. When the PAMS-TVOC level at F4 increased as the wind turned southwesterly, the contribution from the two petrochemical factors also abruptly increased, as shown in Fig. 6b.

Note that in this case the biogenic profile can be extracted out by PMF (Fig. 3S (f)) which is absent under NEM in cold season, because the SWM wind flow mostly occurs in summer when the atmospheric abundance of an iconic biogenic species, isoprene, enhanced significantly (Chang et al., 2014; Chang et al., 2005; Yang et al., 2005). As for site F2 and F9, four factors of aged, industrial/

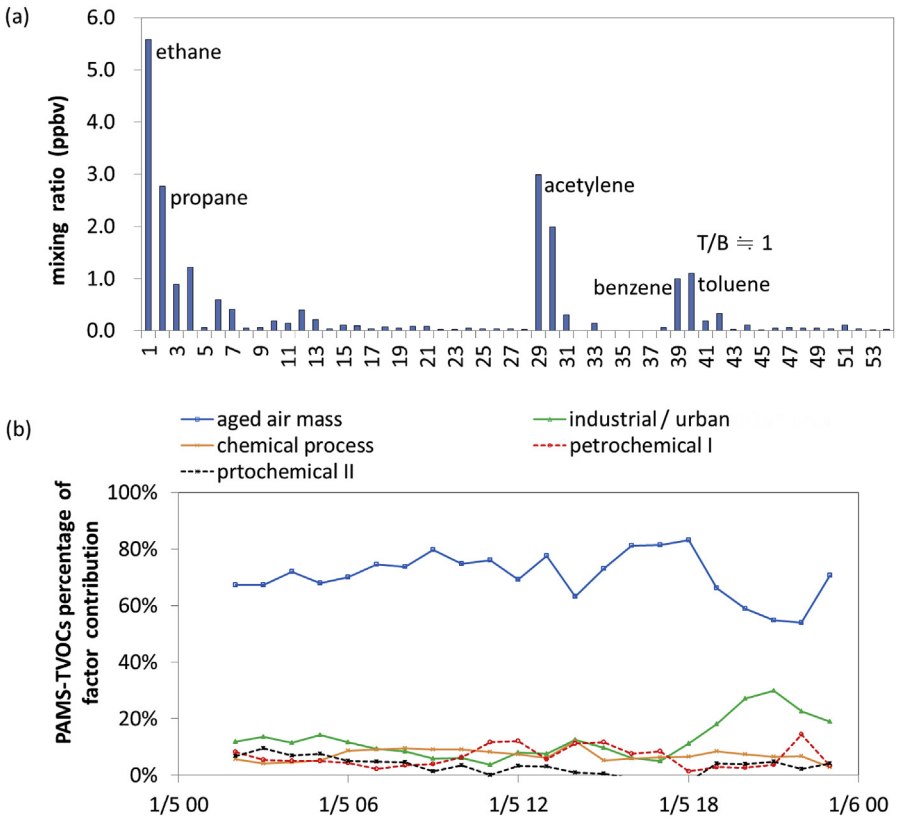

Fig. 5. (a) Observed PAMS profile at site F2 for a typical case of NEM flows described by Fig. 4, which is similar to the PMF profile A in Fig. 2; (b) Percent PAMS-TVOCs with time for the 5 factors, showing dominance by the factor of aged air mass.

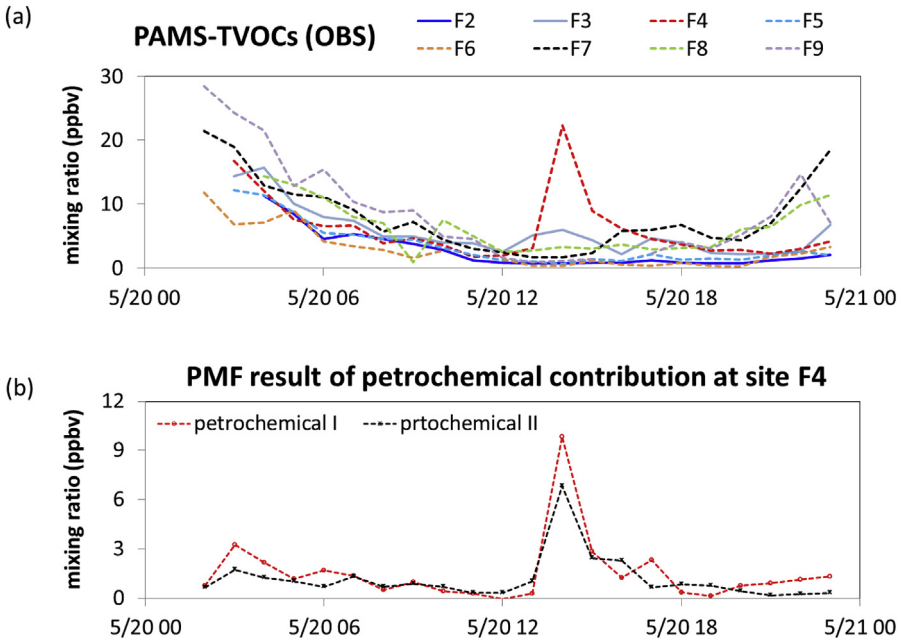

Fig. 6. A typical case of petro-emissions affecting site F4 under SWM flows. (a) PAMS-TVOC observations at eight PAMS sites with site F4 showing an elevated signal in early afternoon of 5/20; (b) petrochemical contributions resolved from PMF at site F4 showing the abrupt rise in petrochemical signals resolved by PMF synchronized with (a).

urban, exhaust/fuel evaporative and biogenic signatures were resolved. The lacks of petrochemical and local painting signals suggest that those areas were less influenced by the Petro-complex and more by other source types during the SWM season.

3.3. LCD flows

Land-sea breezes are often associated with monsoon and manifested by considerably varied wind direction within one day. The LCD flows pattern accounts for 29% days of a year. It is slightly less than the NEM flows that accounts for 37% of the year. The source-receptor relationship varies rapidly within a time frame of only a few hours. With this wind pattern, influences from the Petro-complex are known to be significantly less for the inland area than the coastal (Chen et al., 2018; Su et al., 2016). Five PMF factors of aged air mass (similar to profile A), industrial/urban (similar to profile B), petrochemical-I and petrochemical-II (similar to profile D and E), as well as exhaust/fuel evaporation (similar to profile I) were detected by PMF at F2, F4 and F9 (results are not shown to avoid redundancy).

3.4. Additional tool of validation by effective indicators

In our previous study, the ratios of ethylene/acetylene (E/A) and propylene/acetylene (P/A) were used as effective indicators to reveal the downwind characteristics resulted from the petro-chemical emissions in the Petro-region (Su et al., 2016). We found that the PMF results were in good agreement with the petro-chemical indicators. In Fig. S6 the highly variable features in the petrochemical signatures resolved by PMF (Fig. S6a) match those of E/A and P/A ratios (Fig. S6b). In the calm periods, as circled by the dashed boxes, the VOC abundance was largely contributed by air parcels coming from afar and can be deemed the baseline condition to pose a contrast to the other periods with elevated Petro-emission signals. As a result, the use of effective markers can be deemed as internal references to check or quality-control the robustness of the PMF results. In another words, as distinct and pronounced as the petro-signals, they should be easily revealed by PMF not only with regards to the S/N level, but also to the time of occurrence.

4. Quantitative estimates of source contributions

Our ultimate goal of PMF analysis is to quantify the effect of any given source on the receptor, particularly using the Petro-complex as a showcase to illustrate its effect on downwind areas in a quantitative way. With that in mind, we then further calculated the contributions of the PMF resolved source types to the total observed PAMS-TVOCs at the receptor sites. Under NEM, profiles of petrochemical emissions (petrochemical I and II combined) can be extracted out only at site F2, whereas under SWM the petro-chemical emissions can be extracted out only at site F4. Under LCD, petrochemical emissions can be found at all three sites of F2, F4 and F9 because of the varied wind conditions.

Fig. 7 a ~ c shows the percent contributions to the observed PAMS-TVOCs at three sites of F2, F4 and F9 from individual source types. Under NEM (in Fig. 7a), the aged air mass from afar is the most dominant contribution to the three sites accounting for 37–44% of the observed PAMS-TVOC mixing ratios. The industrial/urban emissions account for 23–31%, followed by the exhaust/fuel evaporation of approximately 23–24% found at F4 and F9, and negligible amount at F2. The solvent/chemical emissions account for 7–9% for the three sites. The petro-chemical emissions I and II combined contribute 26% at site F2, and negligible amount at F4 and F9. F2 was the most petro-affected site. This finding suggests that under NEM which persists as long as 4–5 months in cold season, the region is not significantly affected by the Petro-complex, but by other sources. The impact of the petrochemical emissions was mainly confined within a narrow corridor along the coastal area. Although the Petro-complex appears to be the single largest emission source within the Petro-region, its true impact is greatly alleviated by the NEM wind characteristics.

Under SWM (Fig. 7b), the influence of long-distant aged air is still significant, accounting for 35–38% at the three sites. The industrial/urban decreases to 15–20%. Nevertheless, the exhaust/fuel

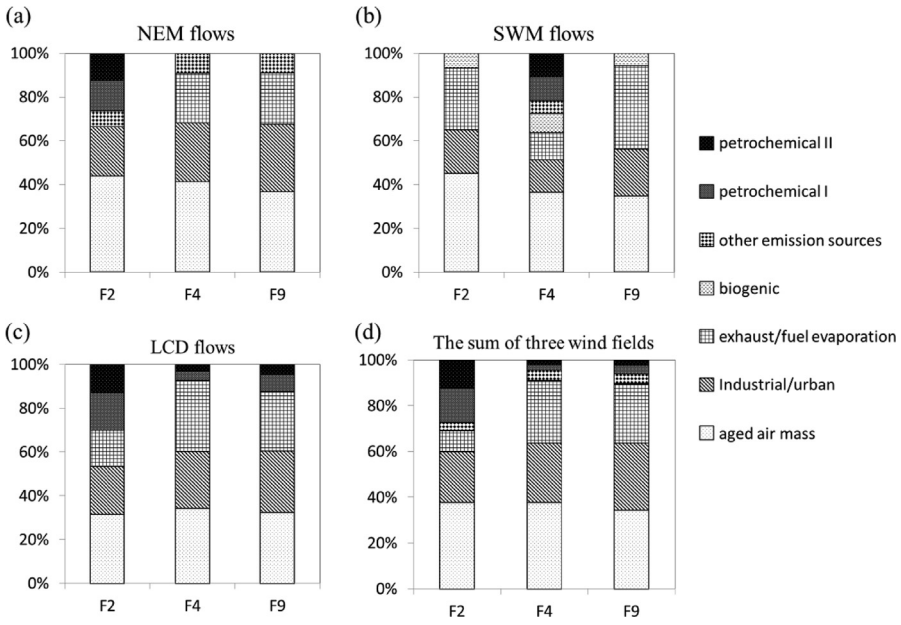

Fig. 7. Source contributions to PAMS-TVOC mixing ratios (in ppbv) at site F2, F4, and F9 under (a) NEM flows; (b) SWM flows; (c) LCD flows; (d) sum over the whole year for the three wind fields.

evaporation increases to 38% at site F9, which means that the inland area is more affected by the traffic source and almost none by Petro-complex. At site F4, which is now the downstream site of the Petro-complex, receives 20% of the petrochemical emissions. Note that all monitoring sites ubiquitously receive biogenic emissions as signified by the measured compound of isoprene, accounting for 6–9% throughout the Petro-region, which is not surprising since SWM prevails in summer when the biogenic emission is most thriving of the year (Chang et al., 2014; Hsieh et al., 2017).

In the LCD wind field (Fig. 7c), the percent contribution of the long-range aged air mass is still the highest (32–34%). The industrial/urban emissions account for 22–28%. Exhaust/fuel evaporation is 17–33%. The urban influence increased significantly under this wind field. The contributions of petrochemical emissions (petrochemical I and II combined) account for 30%, 7%, and 12% respectively at site F2, F4, and F9. Interestingly, site F9, despite its farther distance from the Petro-complex, was significantly more affected by petrochemical emissions than site F4. This is because the probability of northwest wind is twice of that of the southwest wind under LCD in the Petro-region.

We further calculated the percent contribution of a specific source type to the three sites in Petro-region for the whole year by summing over its occurrence under the three wind fields to yield an annual representation:

$$\text{Contribution}(\%)\ \text{of x emission} = \frac{\sum_{i}^{a} G_{xi} \times F_x + \sum_{j}^{b} G_{xj} \times F_x \sum_{k}^{c} G_{xk} \times F_x}{\sum_{i}^{a} \text{PAMS} - \text{TVOCs} + \sum_{j}^{b} \text{PAMS} - \text{TVOCs} + \sum_{k}^{c} \text{PAMS} - \text{TVOCs}}$$

where a, b, and c represent the valid hours of observation data under NEM, SWM and LCD wind field, respectively. F_x represents the source profile x resolved by PMF, G_x represents the hourly contribution for the emission source x, and the PAMS-TVOCs represents the sum of the products of F and G for all emission sources (Fig. 7d). On the yearly basis, the impact of the petrochemical emissions was mainly in the south of the Petro-complex near the coastal area as represented by F2 contributing to about $26 \pm 23\%$ of the observed PAMS-TVOC abundance under the three major wind flow periods which account for nearly 80% of the time in a year. The impact is expected to be slightly higher if the remaining uncounted days were included in assessment. Other sites received much less contributions from the Petro-complex than F2. Although the Petro-complex is the single largest local source, it appears that the Petro-complex's emissions were mostly blown off land to the sea under the NEM flows (Fig. S7). Overall, the Petro-region received much less impact from the Petro-complex's emissions than from other emission types coming from inside or outside the region, which together gave rise to $74 \pm 24\%$ of the observed PAMS-VOCs abundance for the same time period.

5. Conclusions

In this work, we demonstrated the use of PMF analysis to identify major sources of VOCs in a study domain. Its effectiveness can be put to test with the availability of a giant Petrochemical Complex, which can be easily perceived as the single most important contributor of VOCs in the region. Different from the common PMF applications which usually lack effective means of validation, the robustness of PMF results in this work was supported by both model simulations and unique features in time-series observations, which together minimized ambiguity and subjectivity in source assignment. Not only were the overall features and differences between various key sources distinctively resolved, the dynamic changes in contribution of a given source to a receptor were also rationalized, owing to the availability of multispecies time-series observations. Furthermore, with model simulations, the transport of VOC plumes can be visualized to facilitate the understanding of a source-receptor phenomenon with spatial and temporal relevance, which further support the PMF and monitoring results.

Despite the sheer size of the Petro-complex, which may have appeared to be the most significant source of VOCs in the region, its impact on surrounding areas in terms of the contribution of a given source to the total PAMS-TVOC abundance was not as significant as its size implies. Quantitative assessment over an entire year concluded that all sites in the region received far less influence from the Petro-complex than from other emission types within or outside the region, which together add up to 74% of the PAMS-TVOC abundance under three major wind fields.

Conflicts of interest

We declare that we have no financial and personal relationships with other people or organizations that can inappropriately influence our work, there is no professional or other personal interest of any nature or kind in any product, service and/or company that could be construed as influencing the position presented in, or the review of, the manuscript entitled "Source Apportionment of Volatile Organic Compounds (VOCs) by Positive Matrix Factorization (PMF) Supported by Model Simulation and Source Markers - Using Petrochemical Emissions as a Showcase".

Acknowledgments

We thank the Formosa Plastics Group for providing the PAMS monitoring data.

Appendix A. Supplementary data

Supplementary data related to this article can be found at https://doi.org/10.1016/j.envpol.2019.07.016.

References

Atkinson, R., Arey, J., 2003. Atmospheric degradation of volatile organic compounds. Chem. Rev. 103, 4605–4638. https://pubs.acs.org/doi/10.1021/cr0206420.

Brown, S.G., Frankel, A., Hafner, H.R., 2007. Source apportionment of VOCs in the Los Angeles area using positive matrix factorization. Atmos. Environ. 41, 227–237. https://doi.org/10.1016/j.atmosenv.2006.08.021.

Buzcu-Guven, B., Fraser, M.P., 2008. Comparison of VOC emissions inventory data with source apportionment results for Houston, TX. Atmos. Environ. 42, 5032–5043. https://doi.org/10.1016/j.atmosenv.2008.02.025.

Buzcu, B., Fraser, M.P., 2006. Source identification and apportionment of volatile organic compounds in Houston, TX. Atmos. Environ. 40, 2385–2400. https://doi.org/10.1016/j.atmosenv.2005.12.020.

Cai, C., Geng, F., Tie, X., Yu, Q., An, J., 2010. Characteristics and source apportionment of VOCs measured in Shanghai, China. Atmos. Environ. 44, 5005–5014. https://doi.org/10.1016/j.atmosenv.2010.07.059.

Carter, W.P.L., 1990. A detailed mechanism for the gas-phase atmospheric reactions of organic compounds. Atmos. Environ. Part A. General Topics 24, 481–518. https://doi.org/10.1016/0960-1686(90)90005-8.

Carter, W.P.L., 1994. Development of ozone reactivity scales for volatile organic compounds. Air Waste 44, 881–899. https://doi.org/10.1080/1073161X.1994.10467290.

Cetin, E., Odabasi, M., Seyfioglu, R., 2003. Ambient volatile organic compound (VOC) concentrations around a petrochemical complex and a petroleum refinery. Sci. Total Environ. 312, 103–112. https://doi.org/10.1016/S0048-9697(03)00197-9.

Chan, L.-Y., Chu, K.-W., Zou, S.-C., Chan, C.-Y., Wang, X.-M., Barletta, B., Blake, D.R., Guo, H., Tsai, W.-Y., 2006. Characteristics of nonmethane hydrocarbons (NMHCs) in industrial, industrial-urban, and industrial-suburban atmospheres of the Pearl River Delta (PRD) region of south China. J. Geophys. Res. Atmos. 111, D11304. https://doi.org/10.1029/2005JD006481.

Chang, C.-C., Wang, J.-L., Candice Lung, S.-C., Chang, C.-Y., Lee, P.-J., Chew, C., Liao, W.-C., Chen, W.-N., Ou-Yang, C.-F., 2014. Seasonal characteristics of biogenic and anthropogenic isoprene in tropical–subtropical urban environments. Atmos. Environ. 99, 298–308. https://doi.org/10.1016/j.atmosenv.2014.09.019.

Chang, K.-H., Chen, T.-F., Huang, H.-C., 2005. Estimation of biogenic volatile organic compounds emissions in subtropical island—Taiwan. Sci. Total Environ. 346, 184–199. https://doi.org/10.1016/j.scitotenv.2004.11.022.

Chen, M.-H., Yuan, C.-S., Wang, L.-C., 2014a. Source identification of VOCs in a petrochemical complex by applying open-path fourier transform infrared spectrometry. Aerosol. Air Qual. Res. 14, 1630–1638. http://www.aaqr.org/doi/10.4209/aaqr.2014.04.0079.

Chen, S.-P., Liao, W.-C., Chang, C.-C., Su, Y.-C., Tong, Y.-H., Chang, J.S., Wang, J.-L., 2014b. Network monitoring of speciated vs. total non-methane hydrocarbon measurements. Atmos. Environ. 90, 33–42. https://doi.org/10.1016/j.atmosenv.2014.03.020.

Chen, S.-P., Liu, T.-H., Chen, T.-F., Yang, C.-F.O., Wang, J.-L., Chang, J.S., 2010. Diagnostic modeling of PAMS VOC observation. Environ. Sci. Technol. 44, 4635–4644. https://doi.org/10.1021/es903361r.

Chen, S.-P., Liu, W.-T., Ou-Yang, C.-F., Chang, J.S., Wang, J.-L., 2014c. Optimizing the emission inventory of volatile organic compounds (VOCs) based on network observations. Atmos. Environ. 84, 1–8. https://doi.org/10.1016/j.atmosenv.2013.10.059.

Chen, S.-P., Su, Y.-C., Chiu, C.-J., Lin, C.-H., Chang, J.S., Chang, C.-C., Wang, J.-L., 2015. Inter-comparison of network measurements of non-methane organic compounds with model simulations. Atmos. Environ. 122, 94–102. https://doi.org/10.1016/j.atmosenv.2015.09.033.

Chen, S.-P., Wang, C.-H., Lin, W.-D., Tong, Y.-H., Chen, Y.-C., Chiu, C.-J., Chiang, H.-C., Fan, C.-L., Wang, J.-L., Chang, J.S., 2018. Air quality impacted by local pollution sources and beyond – using a prominent petro-industrial complex as a study case. Environ. Pollut. 236, 699–705. https://doi.org/10.1016/j.envpol.2018.01.091.

Cooper, J.A., Watson, J.G., 1980. Receptor oriented methods of air particulate source apportionment. J. Air Pollut. Control Assoc. 30, 1116–1125. https://doi.org/10.1080/00022470.1980.10465157.

Dumanoglu, Y., Kara, M., Altiok, H., Odabasi, M., Elbir, T., Bayram, A., 2014. Spatial and seasonal variation and source apportionment of volatile organic compounds (VOCs) in a heavily industrialized region. Atmos. Environ. 98, 168–178. https://doi.org/10.1016/j.atmosenv.2014.08.048.

Formosa Plastics Group, 2013. Formosa Plastics Group 2013 Annual Report.

Gelencsér, A., Siszler, K., Hlavay, J., 1997. Toluene–Benzene concentration ratio as a tool for characterizing the distance from vehicular emission sources. Environ. Sci. Technol. 31, 2869–2872. https://doi.org/10.1021/es970004c.

Guo, H., Cheng, H.R., Ling, Z.H., Louie, P.K.K., Ayoko, G.A., 2011. Which emission sources are responsible for the volatile organic compounds in the atmosphere of Pearl River Delta? J. Hazard Mater. 188, 116–124. https://doi.org/10.1016/j.jhazmat.2011.01.081.

Hajizadeh, Y., Teiri, H., Nazmara, S., Parseh, I., 2018. Environmental and biological monitoring of exposures to VOCs in a petrochemical complex in Iran. Environ. Sci. Pollut. Res. 25, 6656–6667. https://link.springer.com/article/10.1007/s11356-017-1045-4.

Han, D., Gao, S., Fu, Q., Cheng, J., Chen, X., Xu, H., Liang, S., Zhou, Y., Ma, Y., 2018. Do volatile organic compounds (VOCs) emitted from petrochemical industries affect regional PM2.5? Atmos. Res. 209, 123–130. https://doi.org/10.1016/j.atmosres.2018.04.002.

Ho, K.F., Lee, S.C., Ho, W.K., Blake, D.R., Cheng, Y., Li, Y.S., Ho, S.S.H., Fung, K., Louie, P.K.K., Park, D., 2009. Vehicular emission of volatile organic compounds (VOCs) from a tunnel study in Hong Kong. Atmos. Chem. Phys. 9, 7491–7504. https://doi.org/10.5194/acp-9-7491-2009.

Hsieh, H.-C., Ou-Yang, C.-F., Wang, J.-L., 2017. Revelation of coupling biogenic with anthropogenic isoprene by highly time-resolved observations. Aerosol. Air Qual. Res. 17, 721–729. http://www.aaqr.org/article/detail/AAQR-16-04-OA-0133.

Hsu, C.-Y., Chiang, H.-C., Shie, R.-H., Ku, C.-H., Lin, T.-Y., Chen, M.-J., Chen, N.-T., Chen, Y.-C., 2018. Ambient VOCs in residential areas near a large-scale petrochemical complex: spatiotemporal variation, source apportionment and health risk. Environ. Pollut. 240, 95–104. https://doi.org/10.1016/j.envpol.2018.04.076.

Hwa, M.-Y., Hsieh, C.-C., Wu, T.-C., Chang, L.-F.W., 2002. Real-world vehicle emissions and VOCs profile in the Taipei tunnel located at Taiwan Taipei area. Atmos. Environ. 36, 1993–2002. https://doi.org/10.1016/S1352-2310(02)00148-6.

Jobson, B.T., Berkowitz, C.M., Kuster, W.C., Goldan, P.D., Williams, E.J., Fesenfeld, F.C., Apel, E.C., Karl, T., Lonneman, W.A., Riemer, D., 2004. Hydrocarbon source signatures in Houston, Texas: influence of the petrochemical industry. J. Geophys. Res. Atmos. 109, D24305. https://doi.org/10.1029/2004JD004887.

Jones, A.P., 1999. Indoor air quality and health. Atmos. Environ. 33, 4535–4564. https://doi.org/10.1016/S1352-2310(99)00272-1.

Kuo, C.-P., Liao, H.-T., Chou, C.C.K., Wu, C.-F., 2014. Source apportionment of particulate matter and selected volatile organic compounds with multiple time resolution data. Sci. Total Environ. Environ. 472, 880–887. https://doi.org/10.1016/j.scitotenv.2013.11.114.

Lau, C., Fiedler, H., Hutzinger, O., Schwind, K.H., Hosseinpour, J., 1997. Levels of selected organic compounds in materials for candle production and human exposure to candle emissions. Chemosphere 34, 1623–1630. https://doi.org/10.1016/S0045-6535(97)00458-X.

Leuchner, M., Rappenglück, B., 2010. VOC source–receptor relationships in Houston during TexAQS-II. Atmos. Environ. 44, 4056–4067. https://doi.org/10.1016/j.atmosenv.2009.02.029.

Li, M., Zhang, Q., Streets, D.G., He, K.B., Cheng, Y.F., Emmons, L.K., Huo, H., Kang, S.C., Lu, Z., Shao, M., Su, H., Yu, X., Zhang, Y., 2014. Mapping Asian anthropogenic emissions of non-methane volatile organic compounds to multiple chemical mechanisms. Atmos. Chem. Phys. 14, 5617–5638. https://doi.org/10.5194/acp-14-5617-2014.

Liao, H.-T., Kuo, C.-P., Hopke, P.K., Wu, C.-F., 2013. Evaluation of a modified receptor model for solving multiple time resolution equations: a simulation study. Aerosol. Air Qual. Res. 13, 1253–1262. http://www.aaqr.org/article/detail/AAQR-12-11-OA-0322.

Lin, C.H., 2012. 2008 Gridded Land-Use Database in Taiwan.

Liu, W.-T., Chen, S.-P., Chang, C.-C., Ou-Yang, C.-F., Liao, W.-C., Su, Y.-C., Wu, Y.-C.,

Wang, C.-H., Wang, J.-L., 2014. Assessment of carbon monoxide (CO) adjusted non-methane hydrocarbon (NMHC) emissions of a motor fleet – a long tunnel study. Atmos. Environ. 89, 403–414. https://doi.org/10.1016/j.atmosenv.2014.01.002.

McCarthy, M.C., Aklilu, Y.-A., Brown, S.G., Lyder, D.A., 2013. Source apportionment of volatile organic compounds measured in Edmonton, Alberta. Atmos. Environ. 81, 504–516. https://doi.org/10.1016/j.atmosenv.2013.09.016.

McFiggans, G., Mentel, T.F., Wildt, J., Pullinen, I., Kang, S., Kleist, E., Schmitt, S., Springer, M., Tillmann, R., Wu, C., Zhao, D., Hallquist, M., Faxon, C., Le Breton, M., Hallquist, Å.M., Simpson, D., Bergström, R., Jenkin, M.E., Ehn, M., Thornton, J.A., Alfarra, M.R., Bannan, T.J., Percival, C.J., Priestley, M., Topping, D., Kiendler-Scharr, A., 2019. Secondary organic aerosol reduced by mixture of atmospheric vapours. Nature 565, 587–593. https://www.nature.com/articles/s41586-018-0871-y.

Miller, L., Xu, X., Wheeler, A., Atari, D.O., Grgicak-Mannion, A., Luginaah, I., 2011. Spatial variability and application of ratios between BTEX in two Canadian cities. Sci. World J. 11, 2536–2549. https://doi.org/10.1100/2011/167973.

Mo, Z., Shao, M., Lu, S., Qu, H., Zhou, M., Sun, J., Gou, B., 2015. Process-specific emission characteristics of volatile organic compounds (VOCs) from petrochemical facilities in the Yangtze River Delta, China. Sci. Total Environ. 533, 422–431. https://doi.org/10.1016/j.scitotenv.2015.06.089.

Paatero, P., 1997. Least squares formulation of robust non-negative factor analysis. Chemometr. Intell. Lab. Syst. 37, 23–35. https://doi.org/10.1016/S0169-7439(96)00044-5.

Paatero, P., Tapper, U., 1994. Positive matrix factorization: a non-negative factor model with optimal utilization of error estimates of data values. Environmetrics 5, 111–126. https://doi.org/10.1002/env.3170050203.

Pekey, B., Yılmaz, H., 2011. The use of passive sampling to monitor spatial trends of volatile organic compounds (VOCs) at an industrial city of Turkey. Microchem. J. 97, 213–219. https://doi.org/10.1016/j.microc.2010.09.006.

Poirot, R.L., Wishinski, P.R., Hopke, P.K., Polissar, A.V., 2001. Comparative application of multiple receptor methods to identify aerosol sources in northern Vermont. Environ. Sci. Technol. 35, 4622–4636. https://doi.org/10.1021/es010588p.

Ras, M.R., Marcé, R.M., Borrull, F., 2009. Characterization of ozone precursor volatile organic compounds in urban atmospheres and around the petrochemical industry in the Tarragona region. Sci. Total Environ. 407, 4312–4319. https://doi.org/10.1016/j.scitotenv.2009.04.001.

Reff, A., Eberly, S.I., Bhave, P.V., 2007. Receptor modeling of ambient particulate matter data using positive matrix factorization: review of existing methods. J. Air Waste Manag. Assoc. 57, 146–154. https://doi.org/10.1080/10473289.2007.10465319.

Ryerson, T.B., Trainer, M., Angevine, W.M., Brock, C.A., Dissly, R.W., Fehsenfeld, F.C., Frost, G.J., Goldan, P.D., Holloway, J.S., Hübler, G., Jakoubek, R.O., Kuster, W.C., Neuman, J.A., Nicks, D.K., Parrish, D.D., Roberts, J.M., Sueper, D.T., Atlas, E.L., Donnelly, S.G., Flocke, F., Fried, A., Potter, W.T., Schauffler, S., Stroud, V., Weinheimer, A.J., Wert, B.P., Wiedinmyer, C., Alvarez, R.J., Banta, R.M., Darby, L.S., Senff, C.J., 2003. Effect of petrochemical industrial emissions of reactive alkenes and NOx on tropospheric ozone formation in Houston, Texas. J. Geophys. Res. Atmos. 108 (D8), 4249. https://doi.org/10.1029/2002JD003070.

Saeaw, N., Thepanondh, S., 2015. Source apportionment analysis of airborne VOCs using positive matrix factorization in industrial and urban areas in Thailand. Atmos. Pollut. Res. 6, 644–650. https://doi.org/10.5094/APR.2015.073.

Schauer, J.J., Fraser, M.P., Cass, G.R., Simoneit, B.R.T., 2002. Source reconciliation of atmospheric gas-phase and particle-phase pollutants during a severe photochemical smog episode. Environ. Sci. Technol. 36, 3806–3814. https://doi.org/10.1021/es011458j.

Scheff, P.A., Wadden, R.A., 1993. Receptor modeling of volatile organic compounds. 1. Emission inventory and validation. Environ. Sci. Technol. 27, 617–625. https://doi.org/10.1021/es00041a005.

Scheff, P.A., Wadden, R.A., Bates, B.A., Aronian, P.F., 1989. Source fingerprints for receptor modeling of volatile organics. JAPCA 39, 469–478. https://doi.org/10.1080/08940630.1989.10466546.

Seagrave, J., McDonald, J.D., Bedrick, E., Edgerton, E.S., Gigliotti, A.P., Jansen, J.J., Ke, L., Naeher, L.P., Seilkop, S.K., Zheng, M., Mauderly, J.L., 2006. Lung toxicity of ambient particulate matter from southeastern U.S. Sites with different contributing sources: relationships between composition and effects. Environ. Health Perspect. 114, 1387–1393. https://doi.org/10.1289/ehp.9234.

Simpson, I.J., Marrero, J.E., Batterman, S., Meinardi, S., Barletta, B., Blake, D.R., 2013. Air quality in the Industrial Heartland of Alberta, Canada and potential impacts on human health. Atmos. Environ. 81, 702–709. https://doi.org/10.1016/j.atmosenv.2013.09.017.

Stockwell, W.R., Middleton, P., Chang, J.S., Tang, X., 1990. The second generation regional acid deposition model chemical mechanism for regional air quality modeling. J. Geophys. Res. Atmos. 95, 16343–16367. https://doi.org/10.1029/JD095iD10p16343.

Stojić, A., Stanišić Stojić, S., Mijić, Z., Šoštarić, A., Rajšić, S., 2015. Spatio-temporal distribution of VOC emissions in urban area based on receptor modeling. Atmos. Environ. 106, 71–79. https://doi.org/10.1016/j.atmosenv.2015.01.071.

Su, Y.-C., Chen, S.-P., Tong, Y.-H., Fan, C.-L., Chen, W.-H., Wang, J.-L., Chang, J.S., 2016. Assessment of regional influence from a petrochemical complex by modeling and fingerprint analysis of volatile organic compounds (VOCs). Atmos. Environ. 141, 394–407. https://doi.org/10.1016/j.atmosenv.2016.07.006.

Taiwan-EPA, 2011. Taiwan Emission Database System Website. http://teds.epa.gov.tw/new_main2.htm.

Wang, Q., Li, S., Dong, M., Li, W., Gao, X., Ye, R., Zhang, D., 2018. VOCs emission characteristics and priority control analysis based on VOCs emission inventories and ozone formation potentials in Zhoushan. Atmos. Environ. 182, 234–241. https://doi.org/10.1016/j.atmosenv.2018.03.034.

Wei, W., Cheng, S., Li, G., Wang, G., Wang, H., 2014. Characteristics of volatile organic compounds (VOCs) emitted from a petroleum refinery in Beijing, China. Atmos. Environ. 89, 358–366. https://doi.org/10.1016/j.atmosenv.2014.01.038.

Wu, C.-F., Wu, T.-g., Hashmonay, R.A., Chang, S.-Y., Wu, Y.-S., Chao, C.-P., Hsu, C.-P., Chase, M.J., Kagann, R.H., 2014. Measurement of fugitive volatile organic compound emissions from a petrochemical tank farm using open-path Fourier transform infrared spectrometry. Atmos. Environ. 82, 335–342. https://doi.org/10.1016/j.atmosenv.2013.10.036.

Xie, Y., Berkowitz, C.M., 2006. The use of positive matrix factorization with conditional probability functions in air quality studies: an application to hydrocarbon emissions in Houston, Texas. Atmos. Environ. 40, 3070–3091. https://doi.org/10.1016/j.atmosenv.2005.12.065.

Yang, J.-C., Chang, P.-E., Chie, W.-C., Liu, J.-P., Wu, C.-F., 2016. Large-scale search method for locating and identifying fugitive emission sources in petrochemical processing areas. Process Saf. Environ. Prot. 104, 382–394. https://doi.org/10.1016/j.psep.2016.09.015.

Yang, K.-L., Ting, C.-C., Wang, J.-L., Wingenter, O.W., Chan, C.-C., 2005. Diurnal and seasonal cycles of ozone precursors observed from continuous measurement at an urban site in Taiwan. Atmos. Environ. 39, 3221–3230. https://doi.org/10.1016/j.atmosenv.2005.02.003.

Yuan, B., Shao, M., Lu, S., Wang, B., 2010. Source profiles of volatile organic compounds associated with solvent use in Beijing, China. Atmos. Environ. 44, 1919–1926. https://doi.org/10.1016/j.atmosenv.2010.02.014.

Yuan, Z., Zhong, L., Lau, A.K.H., Yu, J.Z., Louie, P.K.K., 2013. Volatile organic compounds in the Pearl River Delta: identification of source regions and recommendations for emission-oriented monitoring strategies. Atmos. Environ. 76, 162–172. https://doi.org/10.1016/j.atmosenv.2012.11.034.

Zhang, Q., Streets, D.G., Carmichael, G.R., He, K.B., Huo, H., Kannari, A., Klimont, Z., Park, I.S., Reddy, S., Fu, J.S., Chen, D., Duan, L., Lei, Y., Wang, L.T., Yao, Z.L., 2009. Asian emissions in 2006 for the NASA INTEX-B mission. Atmos. Chem. Phys. 9, 5131–5153. https://doi.org/10.5194/acp-9-5131-2009.

Zhang, Y., Wang, X., Barletta, B., Simpson, I.J., Blake, D.R., Fu, X., Zhang, Z., He, Q., Liu, T., Zhao, X., Ding, X., 2013. Source attributions of hazardous aromatic hydrocarbons in urban, suburban and rural areas in the Pearl River Delta (PRD) region. J. Hazard Mater. 250–251, 403–411. https://doi.org/10.1016/j.jhazmat.2013.02.023.

Zhang, Y., Wang, X., Zhang, Z., Lü, S., Huang, Z., Li, L., 2015. Sources of C2–C4 alkenes, the most important ozone nonmethane hydrocarbon precursors in the Pearl River Delta region. Sci. Total Environ. 502, 236–245. https://doi.org/10.1016/j.scitotenv.2014.09.024.

Zhou, X., Li, Z., Zhang, T., Wang, F., Wang, F., Tao, Y., Zhang, X., Wang, F., Huang, J., 2019. Volatile organic compounds in a typical petrochemical industrialized valley city of northwest China based on high-resolution PTR-MS measurements: characterization, sources and chemical effects. Sci. Total Environ. 671, 883–896. https://doi.org/10.1016/j.scitotenv.2019.03.283.